Nucleon inelastic scattering cross sections on ^{16}O and ^{28}Si

M. Boromiza, C. Borcea, P. Dessagne, D. Ghita, T. Glodariu, G. Henning, M. Kerveno, N. Marginean, C. Mihai, R. Mihai, et al.

Nucleon inelastic scattering cross sections on ^{16}O and ^{28}Si

M. Boromiza,[1,*] C. Borcea,[1] P. Dessagne,[2,3] I. Dinescu,[1] D. Ghita,[4] T. Glodariu †,[1] G. Henning,[2,3] M. Kerveno,[2,3] N. Marginean,[1] C. Mihai,[1] R. Mihai,[1] A. Negret,[1] C. Nita,[1] M. Nyman,[5] A. Olacel,[1] A. Oprea,[1] A.J.M. Plompen,[5] C. Sotty,[1] G. Suliman,[4] R. Suvaila,[1] L. Stan,[1] A. Turturica,[1] and G. Turturica[4]

[1] *Horia Hulubei National Institute for Physics and Nuclear Engineering, Reactorului 30,* 077125 *Bucharest-Măgurele, Romania*
[2] *Université de Strasbourg, IPHC, 23 Rue du Loess, 67037, Strasbourg, France*
[3] *CNRS, UMR7178, 67037, Strasbourg, France*
[4] *Horia Hulubei National Institute for Physics and Nuclear Engineering, ELI-NP, Reactorului 30,* 077125 *Bucharest-Măgurele, Romania*
[5] *European Commission, Joint Research Centre, Retieseweg 111, B − 2440 Geel, Belgium*

(Dated: September 13, 2019)

This paper reports cross section measurements of the (n, n') and (p, p') reactions on ^{16}O and ^{28}Si at GELINA (Geel Electron LINear Accelerator) and at the 9-MV Tandem Accelerator of IFIN-HH (Horia Hulubei National Institute for Physics and Nuclear Engineering), respectively.

The main purpose was to measure the neutron- and proton-induced inelastic γ-production cross sections, for all observed transitions in ^{16}O and ^{28}Si, followed by the calculation of the corresponding total inelastic cross section. The results are compared with theoretical calculations performed using the TALYS 1.9 code, evaluated nuclear data and with previously reported experimental data.

The broader goal of this work is to study if and to which extent the neutron-induced inelastic cross sections of these nuclei can be inferred from those obtained using suitable charged particle reactions. We show that, by making use of the formal similarities between the neutron- and the proton-target optical model potentials and isospin symmetry in mirror nuclei, one can develop a procedure that combines experimental proton-induced inelastic cross sections with theoretical calculations to infer neutron inelastic cross sections. For ^{16}O and ^{28}Si, the precision associated with this procedure is around 10-20% for most of the incident energy range.

PACS numbers: 25.40.Fq, 27.40.+z, 29.30.Kv

I. INTRODUCTION

Considering the serious ecological threat associated to the energy production based on fossil fuels, the nuclear option will most likely play an important role in the decades to come. Nuclear energy has its own challenges to be surpassed, such as safety, economic efficiency and the danger of proliferation. Also, more advanced nuclear technologies are needed to better address the limited fissile fuel and nuclear waste issues.

In this regard, the community aims at developing a new generation of nuclear reactors (i.e. Generation IV fast reactors) that will use fuel which is much more abundant. In such facilities the minor actinides - resulted from the neutron capture and/or decay of the primary fission products - may be recycled as part of the fuel. From a technological point of view, one of the main drawbacks in the construction of these new reactors is that serious improvements are required in both the range and the precision of the existing neutron cross section databases, especially for fast neutrons. In particular, this requirement also applies to the inelastic channel.

Oxygen has three stable isotopes, with ^{16}O being the most abundant (99.75% [1]). Its presence in oxide reactor fuels and water and, by forming oxides, also as a structural material of nuclear reactors make it one of the most important isotopes under the focus of the CIELO collaboration [2] and the High Priority Request List (HPRL) of the Nuclear Energy Agency (NEA) [3].

The dominant heating inside a nuclear reactor results from the fission γ rays and from the neutron and fission fragments slowdown. Therefore, measuring the γ rays emitted by excited ^{16}O nuclei following neutron inelastic scattering results in a better understanding of the neutron slowdown mechanism and also of the γ-rays sources inside the reactor.

The proton-induced inelastic reactions on ^{16}O and ^{28}Si are also of importance. In the case of ^{16}O, there is a single data set providing angle-integrated γ-production cross section for the secondary transitions [4]. No data exists below 8-MeV incident energy and there are some discrepancies between the already measured quantities [4, 5]. The angle-integrated γ-production cross section data for proton inelastic scattering on ^{28}Si is scarce. There is a single data set provided by Marchand *et al.* [6], in a limited incident energy range (3.5-6.6 MeV) and only for the first transition. No angle-integrated γ-production cross sections for the secondary ^{28}Si transitions exist [5]. In the present work, we report proton-induced cross section points in a wide energy range (6-17 MeV) on both ^{16}O and ^{28}Si (see Section IV).

An important motivation for concomitantly investigating the neutron- and the proton-induced inelastic reactions on the same nucleus is related to our study on the

* marian.boromiza@nipne.ro

possibility of inferring the neutron inelastic cross section from the corresponding proton-induced one.

Numerous attempts were made in the past using the so-called *surrogate method* [7–14] producing encouraging results in several particular cases for neutron capture and fission reactions or, more recently, for the (n, p) channel [15]. This method involves the production of the nucleus that undergoes fission or γ decay through a direct reaction induced by a high-energy charged particle. The approach we undertake is essentially different from the conventional surrogate method, but the broader context of this work is to study the potential use of a similar idea for the inelastic channel.

The neutron inelastic scattering cross sections on ^{28}Si were already measured very precisely by our group and the results have been published in Ref. [16]. In that article, a comparison is also made between the ^{28}Si(n, nγ)^{28}Si and ^{25}Mg(α, nγ)^{28}Si reactions. Bohr's hypothesis assumes that the input and the output channels are independent if the nuclear reaction proceeds through a compound nucleus (CN) [17]. Considering that the above two reactions have identical compound nuclei and exit channels, in a simple interpretation of Bohr's hypothesis, one could expect similar shapes and/or absolute values of the γ-production cross sections extracted in the two cases.

Continuing on the same line of thought, in the present work we investigate two pairs of nuclear reactions: ^{16}O(n, nγ)^{16}O versus ^{16}O(p, pγ)^{16}O and similarly for the ^{28}Si target. This time, instead of proceeding through the same compound nucleus as in the case above, two pairs of mirror compound nuclei are formed: ^{17}O-^{17}F and ^{29}Si-^{29}P for the ^{16}O and the ^{28}Si targets, respectively. We chose $N = Z$ targets in order to maximize the effects of the isospin symmetry. Given the structural similarity of mirror nuclei and the similarity between the proton- and neutron-target optical model potentials (OMPs), the two corresponding neutron- versus proton-induced γ-production cross sections may be comparable or even proportional. Section V discusses these points in detail by presenting a procedure able to relate the proton-induced inelastic cross section to the neutron-induced one with reasonable precision.

II. EXPERIMENTAL SETUPS AND PARTICULARITIES

A. The GELINA neutron source and the GAINS spectrometer of EC-JRC

The GELINA neutron source, where the GAINS spectrometer is located, is described in Refs. [18–21]. GELINA consists of a linear accelerator shooting an intense, 70-140 MeV pulsed electron beam on a depleted uranium target. The duration of the pulses is around 1 ns and the repetition rate is 800 Hz. Following the bremsstrahlung radiation, the neutrons are mainly produced by (γ, n) and (γ, fission) reactions. The incident neutron energy is determined via the time-of-flight technique. Several flight paths are available. For the present experiment we used the cabin located at a distance of 200 m from the neutron source. The experiment made use of a very thick [32.30(4) mm] SiO_2 sample with a diameter of 76.26(4) mm. It was irradiated for a total of 472 h ($\approx$ 19 days of continuous measurement). The γ rays emitted by the excited target nuclei were detected employing the GAINS spectrometer (see Fig. 1). In the present experiment twelve HPGe detectors were in use. The detectors have a 100% relative efficiency and were placed at distances of $\approx$ 17.5 cm from the sample. They were read-out by ACQIRIS digitizers with a sampling frequency of 420 MHz and an amplitude range of 12 bits. A fission chamber with ^{235}U deposits was used for incident flux monitoring [22]. The signals coming from the chamber were collected using conventional electronics.

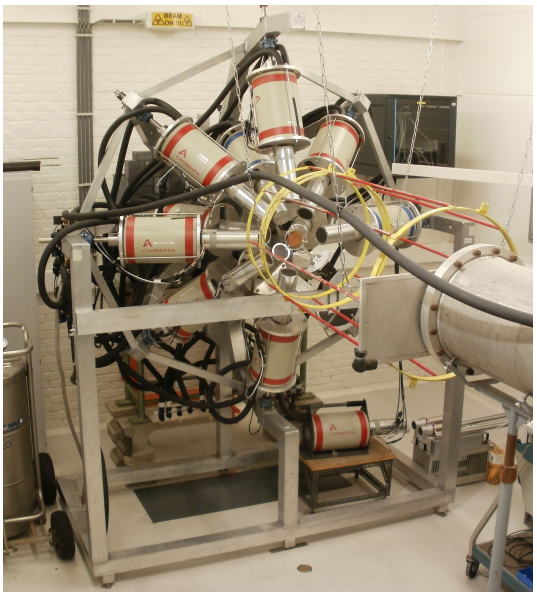

FIG. 1. (Color online) The GAINS spectrometer used during the neutron-induced experiment. It is located in the 200-m measurement cabin and consists of twelve HPGe detectors placed at backward angles (110°, 125° and 150°) in order to minimize the effect of the γ-flash photons scattered on our sample.

B. The 9-MV Tandem accelerator of IFIN-HH and the HPGe detection system

The (p, pγ) experiment was performed at the 9-MV Tandem facility of the Horia Hulubei National Institute for Physics and Nuclear Engineering (IFIN-HH), Bucharest-Măgurele [23, 24]. The incident protons had energies ranging from 6 to 17 MeV, with 1-MeV steps, and they were scattered by a thick [0.195(2) mm or 42.93(45) mg/cm^2] SiO_2 target. A Faraday cup was

placed after the target, as close as possible, in order to collect the protons that passed through (see Fig. 2). The detection system consisted of two HPGe detectors with 100% relative efficiency, placed at 150° (D1) and 110° (D2) relative to the proton beam direction and at around 15.45 cm and 18.25 cm from the target, respectively. The data acquisition consisted of TNT2 cards [25] with 14-bits for amplitude resolution which digitized the continuous signals provided by the preamplifiers with a sampling frequency of 100 MHz. The FPGA board of the TNT2 performs online digital signal processing, avoiding the transfer of the sampled signals to the PC for analysis. This feature allowed working even at relatively high counting rates.

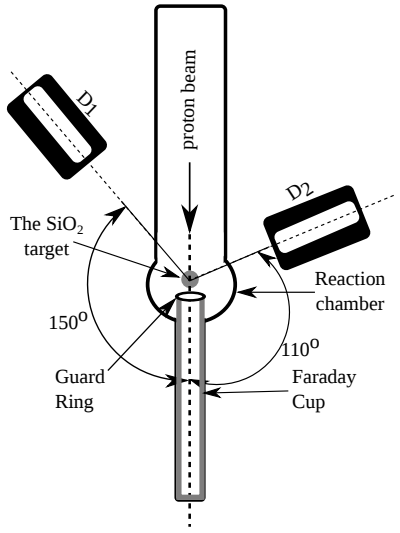

FIG. 2. A schematic drawing of the experimental setup used during our (p, pγ) experiment. It depicts the two detector positions, the reaction chamber and the Faraday cup. The cup was placed at the back of the reaction chamber to collect the protons that passed through the target during the measurement.

C. Experimental particularities and difficulties

Because in the experiments reported here the γ energies of interest span over a large range (the main transitions in ^{28}Si and ^{16}O have an energy of 1778.9 keV and 6128.6 keV, respectively), we had to extrapolate the detector efficiency up to about 7 MeV. In both experiments, this was done using an experimental efficiency curve, obtained via a ^{152}Eu calibration source, followed by MCNP6 simulations [19, 26].

Special care had to be taken due to the thick targets used in our experiments.

In the proton-induced experiment, the energy loss inside the target could not be neglected. We assumed a constant stopping power over the thickness of the target as even the lowest energy protons are far away from the Bragg total absorption peak (the 6-MeV protons lose around 2 MeV). Therefore, we employed the uniform distribution for calculating the average proton energy and its uncertainty after exiting the target. The γ-ray attenuation generated by the reaction chamber was taken into account through the MCNP6 simulations associated to the detector efficiency calibrations.

In the neutron-induced experiment, we had to quantify the γ-ray attenuation inside the thick sample and to calculate the neutron multiple scattering correction factors. The latter refer to those events when the incoming neutron scatters more than once inside the quartz sample. This introduces spurious events where the time of flight (tof) technique no longer allows the determination of the incident energy. Both these effects were quantified based on realistic MCNP6 simulations [27].

During the (p, p') experiment an important issue was the dead time due to high counting rates. Depending on the value of the counting rate in a given experimental run, the dead time correction factor ranged between 3 and 8%. For the detailed correction procedure see Ref. [28]. On the other hand, due to the small incident neutron flux at the 200-m measurement cabin and to the use of triggering conditions that avoid detecting (most of) the very intense γ-flash, in the (n, n') experiment the counting rates were very small (5-10 counts/second per detector). Consequently, the count loss due to dead time was negligible in this case [27, 29].

The 6915.5-, 7115.1- and 2741.5-keV transitions in ^{16}O decay from excited levels with half-lives in the fs range [30]. A TALYS 1.9 [31] reaction kinematics calculation yields an average energy of the ^{16}O recoils of around 200-300 keV, for 0.5-20 MeV incident neutrons (protons). The recoils are stopped inside the quartz target after $\approx$ 2 ps (according to a flight time estimate based on a SRIM calculation [32]). Therefore, practically all the 6915.5-, 7115.1- and 2741.5-keV detected γ rays were emitted by the recoiling nuclei while still moving. In consequence, the γ peaks corresponding to these three transitions were broadened and Doppler-shifted to smaller energies (our detectors being placed at backward angles) with approximatively 15-50 keV, depending on the incident neutron or proton energy. Unfortunately, due to this effect, the 6915.5-keV peak from ^{16}O overlapped with the 6877.0-keV one from ^{28}Si and it was not possible to separate the two contributions in order to extract the cross section of interest. Thus, we will only report their summed contribution (see Section IV).

III. DATA ANALYSIS PROCEDURE

A. The neutron-induced experiment

The data analysis procedure of our experiments performed at the GELINA facility using the GAINS spectrometer was described in Refs. [20, 27, 29, 33]. Here we only mention that the differential cross section was deter-

mined at two angles: 110° and 150° (for cross-checking, also at 125°). These two angles were chosen with the purpose of minimizing the errors made when angularly integrating the differential cross section via the Gaussian quadrature method [cos(110°) and cos(150°) are the nodes of the 4^{th} order Legendre polynomials] [27, 29, 34].

For determining the differential γ-production cross section we used the following expression:

$$\frac{d\sigma_j}{d\Omega}(\theta_i, E_n) = \frac{1}{4\pi} \cdot \frac{Y_j(E_n)}{Y_{FC}(E_n)} \cdot \frac{\varepsilon_{FC}}{\varepsilon_j} \cdot \frac{\rho_U}{\rho_s} \cdot \frac{A_s}{A_U} \cdot \frac{\sigma_U}{c_{ms}(E_n)} \quad (1)$$

where θ_i is the detection angle, E_n is the incident neutron energy, Y_j is the γ yield of the detector j, Y_{FC} is the fission chamber yield, ε_{FC} is the fission chamber efficiency, ε_j is the photopeak efficiency of the detector j, σ_U is the ^{235}U(n, fission) cross section [35], ρ_U is the areal density of the uranium deposits, A_U and A_s are the atomic masses, ρ_s is the areal density of the sample corresponding to the isotope A_s (we had a compound target - SiO_2) and c_{ms} is the neutron multiple scattering correction factor.

After obtaining the differential cross sections at 110° and 150° for each detected transition, the angle-integrated γ-production cross section was calculated using:

$$\sigma(E_n) = 4\pi[w_{110^\circ} \frac{d\sigma}{d\Omega}(110^\circ, E_n) + w_{150^\circ} \frac{d\sigma}{d\Omega}(150^\circ, E_n)] \quad (2)$$

where $\frac{d\sigma}{d\Omega}(110^\circ, E_n)$ and $\frac{d\sigma}{d\Omega}(150^\circ, E_n)$ are the above differential cross sections at 110° and 150°, respectively. The normalisation coefficients $w_{110^\circ} = 0.65214$ and $w_{150^\circ} = 0.34786$ are calculated by solving the system of equations resulting from a series expansion of the differential cross section in the Legendre polynomials algebraic basis [27, 29, 34].

Using the angle-integrated γ-production cross section from Eq. (2) as our primary-extracted quantity, we also calculate the total inelastic cross section by simply adding the cross section of the transitions that decay directly to the ground state - with the correct weighting factors based on the known branching ratios from Refs. [30] and [36].

B. The proton-induced experiment

In the second experiment we used similar γ-spectroscopy techniques in order to extract proton inelastic scattering *absolute* γ-production cross sections. Indeed, the proton-induced data was not measured relatively to a reference cross section, as in the neutron-induced experiment where the ^{235}U(n, fission) cross section was employed. Instead, by collecting the protons that pass through the target, a Faraday cup was used to integrate the beam current and to extract information about the incident proton flux. Also, by analysing the data collected by the detectors we constructed the amplitude spectra for each incident proton energy (see Fig. 3). In these spectra, the γ peaks of interest both from ^{16}O and ^{28}Si were identified and then integrated.

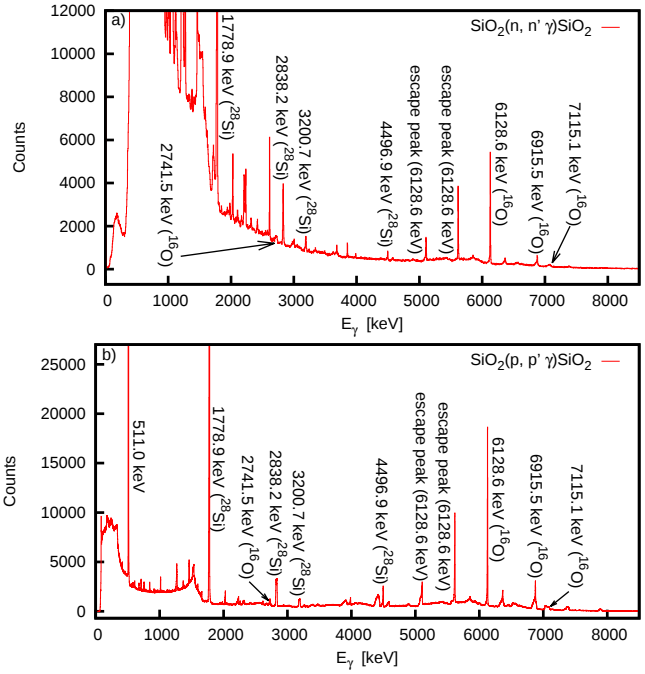

FIG. 3. (Color online) The amplitude spectra associated to the two experiments presented in this work. Both spectra were recorded by a detector placed at 150°. The most intense transitions are identified. One can clearly notice the similarity between the neutron- and proton-induced γ-ray spectra (see the discussion on this point given in Section V).

The differential cross sections at 110° and 150° were determined using the expression:

$$\frac{d\sigma}{d\Omega}(\theta_i, E_p) = \frac{1}{4\pi} \cdot \frac{N_\gamma(\theta_i, E_p) \cdot A_s}{N_p(E_p) \cdot \varepsilon_j \cdot \rho_s} \cdot d \quad (3)$$

where θ_i is the detection angle, E_p is the incident proton energy, N_γ is the integrated number of counts from a given γ peak, N_p is the number of protons incident on the target, ε_j is the efficiency of detector j, A_s is the atomic mass, ρ_s is the areal density of the target corresponding to the isotope A_s and, finally, d is the dead time correction factor (this factor was calculated using the method presented in Ref. [28]).

The angular integration of these differential cross sections is identical with the one presented for the neutron-induced experiment - using Eq. (2) - the detection angles being the same. For other details of the data analysis procedure associated to this experiment see Ref. [37].

C. Uncertainties

Considering the high precision we claim, it is important to discuss in more detail the main sources of uncertainty associated to the two measurements reported here.

In the neutron-induced experiment, the main sources of uncertainty were the γ yield (6% for the main ^{16}O transition after the data on all detectors is added), the fission chamber yield (3%) and its efficiency (2%). As it was already mentioned, we used MCNP6 simulations for extrapolating the efficiency of the detectors to high γ energies. Depending on the number of particles included in the simulation, the code's statistical output has a very small uncertainty (typically below 0.5%). However, the activity of our ^{152}Eu calibration source was known with a 1.5% relative uncertainty. Therefore, the MCNP6-provided uncertainty was increased to 2%, mainly due to the uncertainty of the ^{152}Eu source and to account for any potential geometrical effects in the source-detector position. The mass and area of the sample were measured accurately, so the uncertainty of the areal density was only 0.5%. Considering that the SiO_2 sample (and the ^{235}U deposits of the fission chamber) had diameters larger than the neutron beam, an effect from any non-uniformities in the beam profile was avoided.

The uncertainty corresponding to the multiple scattering coefficient and the self-attenuation of the γ rays inside the sample were quantified based only on Monte Carlo simulations. The software generated very small statistical uncertainties for the two quantities ($< 1\%$). Any potential systematic errors introduced by this procedure were reasonably kept under control by constructing the simulated detection geometry as realistic as possible and by validating it through comparisons with the ^{152}Eu experimental efficiency points. Table I lists an overview of the uncertainties discussed in this section.

TABLE I. Sources of uncertainty and their associated values in the present neutron-induced experiment.

Source	Relative uncertainty [%]
efficiency of the HPGe detectors	2
efficiency of the fission chamber	≈ 2
fission cross section of ^{235}U	< 1
areal density of the sample	0.5
thickness of the fission chamber deposits	< 1
multiple scattering correction factor	< 1

In the proton-induced experiment, the uncertainty resulting from the integration of the proton beam (the quantity N_p) was set to 1% considering the high efficiency of the Faraday cup; also, the uncertainty of the atomic mass A_s was negligible. The uncertainty generated by the dead time correction procedure (the d factor) is negligible for reasons explained in Ref. [28]. Therefore, we considered errors propagating only from the target areal density ρ_s (1%), γ peak area N_γ (3-10% - depending on the available statistics) and detector efficiencies ε_j (3%). As it was the case in the (n, n') experiment, the uncertainty of the calibration source activity was added to the statistical uncertainty arising from the simulations, giving a total of 3% for the detector efficiencies.

IV. RESULTS AND DISCUSSION

This section will present the experimental results obtained in the two experiments. We will start with the ^{16}O reaction data (Sections IV A-IV B) and then move on to ^{28}Si (Section IV C). Section IV D presents the neutron-induced cross sections on ^{28}Si, which we regard as a validation measurement. We were able to extract the γ-production cross section for eight transitions: 6128.6, 6915.5, 7115.1 and 2741.5 keV in ^{16}O and 1778.9, 2838.2, 3200.7 and 4496.9 keV in ^{28}Si. The primary γ-production cross sections are further used, combined with information on the level scheme of the target nucleus, to construct total inelastic cross sections.

A. The ^{16}O(n, nγ)^{16}O reaction

Figure 4 displays a partial level scheme of ^{16}O [30]. The first excited level decays through a totally converted E0 transition which could not be detected using the present setup. Given the very low abundance of the other stable oxygen isotopes (see Section I), no γ peaks corresponding to ^{17}O or ^{18}O were observed in our spectra. Also, the ^{17}O(n, 2nγ)^{16}O contaminating contributions in the γ peaks of interest from ^{16}O were completely negligible (^{17}O has an abundance of only 0.038% [1]).

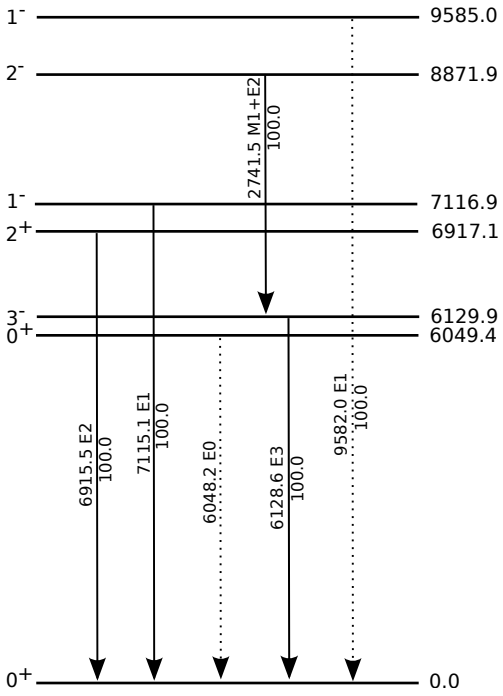

FIG. 4. A partial level scheme of ^{16}O. In the present work we were able to extract, both in the neutron- and in the proton-induced experiments, the cross section for the transitions plotted with a continuous line. The level and γ energies are given in keV.

1. γ-production cross sections

In the following, we will present the production cross section for the observed ^{16}O γ rays: the main transition (6128.6 keV) and the γ rays resulting from higher-lying excited states (6915.5, 7115.1 and 2741.5 keV). They are compared with other experimental data and with TALYS 1.9 theoretical calculations using the default parameters.

The main transition

Figure 5 displays our results for the 6128.6-keV transition in ^{16}O, which is the most intense γ ray in this isotope. The neutron-induced inelastic γ-production cross section values for ^{16}O are scarce. There is a single relatively extended data set available in the literature, with a good incident neutron energy resolution, reported by Nelson *et al.* [38]. When compared with our results, the agreement between the two data sets is very good in the entire incident energy domain (see Fig. 5). The good neutron energy resolution combined with the relatively low level density of ^{17}O, allow the observation of compound nucleus resonances up to very high energies (10-11 MeV) in both cases. Above this incident energy, broader structures are visible. The GELINA neutron source provides a neutron flux with an evaporation spectrum (i.e. maximum intensity around 2-5 MeV) [18]. The authors of Ref. [38] made use of a spallation neutron source, with a high neutron flux mostly for energies above 10-15 MeV. In this respect, the main advantages of the present data, as compared with Nelson *et al.* [38], are given by the much better neutron energy resolution (around 35 keV versus 110 keV at 10 MeV incident energy) and a larger number of cross sections points in the resonance region (below 10 MeV). The two experiments are therefore complementary, as the Nelson *et al.* data have much better statistics at high neutron energies.

The other available experimental results for the main transition [39–41] are within the uncertainty bars in respect to the present work, except the data reported by Dickens *et al.* [39] which lies significantly lower up to 10 MeV incident energy.

Figure 5 also compares the experimental results with theoretical calculations performed with the TALYS 1.9 code, using the default input parameters. Even though the theoretical curve follows the general trend of the experimental cross section, overall, the code underestimates the experimental data (this is particularly true above 15 MeV).

We report the inelastic cross section for the most intense transition in ^{16}O with a total relative uncertainty under 6% for most of the incident energy range (see Fig. 5, panel a).

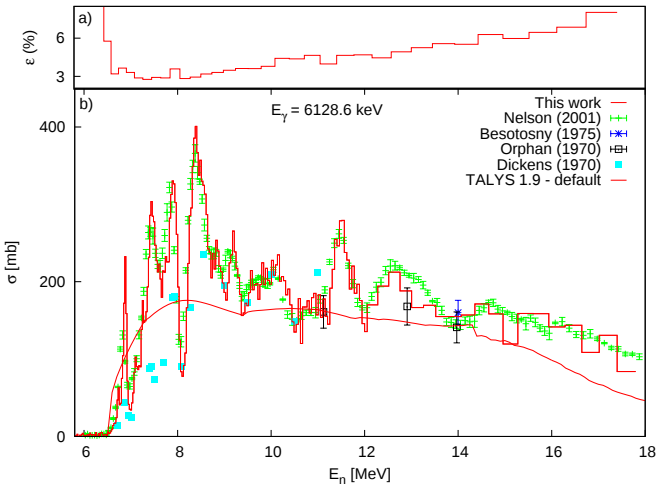

FIG. 5. (Color online) The neutron inelastic angle-integrated γ-production cross section for the 6128.6-keV transition in ^{16}O obtained in the present work (panel b) with its associated relative uncertainty (panel a). It is compared with other available experimental data and with TALYS 1.9 model calculations performed using the default input parameters.

The higher-lying transitions: 6915.5, 7115.1 and 2741.5 keV

Unfortunately, we were not able to extract a clean cross section for the 6915.5-keV transition because - as already mentioned in Section II C - the Doppler shift caused the overlap of the peaks corresponding to the 6915.5-keV (^{16}O) and the 6877.0-keV (^{28}Si) γ rays. Consequently, we report here the cross section for their properly scaled, summed contribution (see Fig. 6). Due to this contaminating contribution coming from ^{28}Si, our 6915.5-keV cross section displays systematically higher values than the ones of Nelson *et al.* We mention that the authors of Ref. [38] did not encounter this issue as their target did not contain silicon. Figure 6 also shows that the experimental data is substantially overestimated by the corresponding TALYS prediction (the red curve).

The same figure also displays our results for the 7115.1- and the 2741.5-keV transitions in ^{16}O. In both cases, Ref. [38] reported cross section points that are slightly higher than ours in the entire incident energy range (especially above 12 MeV) even though the shape is very similar. The TALYS 1.9 prediction for the 7115.1- and the 2741.5-keV transitions is close to the measured values, especially in terms of shape.

Due to their low intensity, we report the cross section for all three higher-lying ^{16}O γ rays with considerably larger total relative uncertainties as compared with the main transition: between 7-12% where the cross section reaches its maximum value and up to 30-40% at 18 MeV.

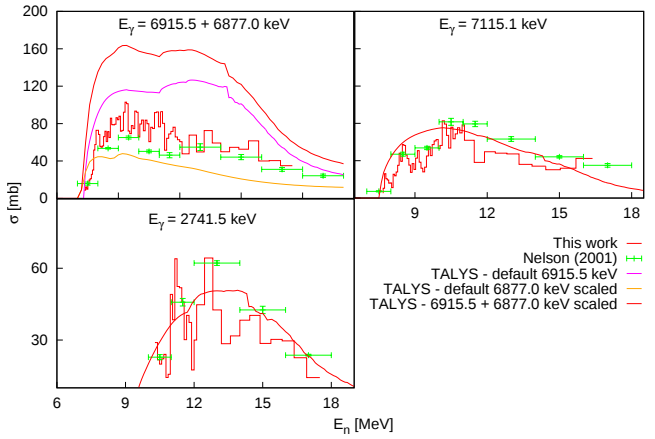

FIG. 6. (Color online) The γ-production cross section for the higher-lying transitions in ^{16}O extracted in the present work compared with TALYS 1.9 theoretical calculations. The data published by Nelson *et al.* is also plotted for all three transitions. Because the 6915.5-keV transition was Doppler shifted to smaller energies ending up on top of the 6877.0-keV transition coming from ^{28}Si (see Section II C), the plot additionally contains the theoretical calculation for this silicon γ ray. The theoretical calculation labelled "TALYS - 6915.5 + 6877.0 keV scaled" represents the properly scaled, summed cross section of the two transitions.

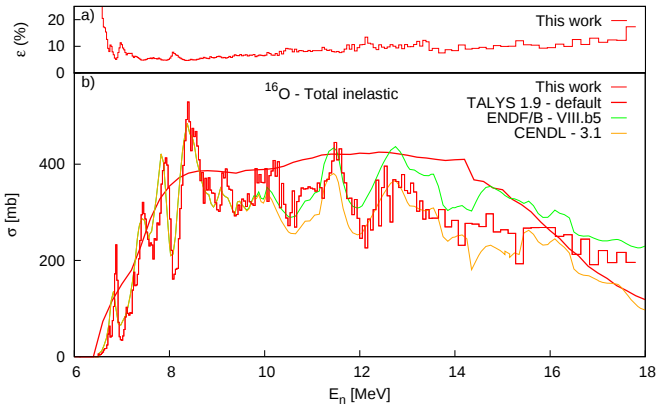

FIG. 7. (Color online) The total inelastic cross section of ^{16}O from the threshold up to 18 MeV obtained in the present work (panel b) with its associated uncertainty (panel a). It is compared with evaluated data taken from ENDF/B - VIII.b5 [42] and CENDL - 3.1 [43] libraries and with TALYS 1.9 model calculations performed using the default input parameters. The JEFF - 3.2 [44] library has identical values with the ENDF/B - VIII.b5, hence it was not plotted here.

2. *Total inelastic cross section*

The neutron-induced total inelastic cross section on ^{16}O was determined by summing the γ-production cross section of all the transitions that decay directly to the ground state: 6128.6, 6915.5 and 7115.1 keV.

As already said, due to Doppler shifts, the cross section of the 6915.5-keV γ ray is contaminated by a contribution coming from the 6877.0-keV transition (^{28}Si), hence so is the ^{16}O total inelastic cross section. Also, we mention that the first ^{16}O transition is totally converted, hence, it was not possible to detect it using the GAINS spectrometer. Therefore, the total inelastic cross section reported here does not include this transition (which has an average cross section of around 25 mb, according to TALYS 1.9).

With these limitations, our results are accurate up to the threshold energy (10.2 MeV) of the first excited level (9585.0 keV) that decays through a γ ray *not* observed by our setup. However, considering that practically all the inelastic strength goes through one of the three γ rays from above (see Fig. 4) and that for excitation energies higher than 10 MeV the γ decay is highly improbable, the total inelastic cross section reported here is close to the real value. Figure 7 plots the results for this quantity as a function of the incident energy. Up to about 9 MeV the evaluated data is able to describe well all the resonant peaks and even some broader structures at higher incident energies. The ENDF/B - VIII.b5 [42] and CENDL - 3.1 [43] evaluations start to diverge above 10 MeV while our data varies somewhat in-between them.

The TALYS calculation, even with the default settings, is able to predict very well the shape of the total inelastic cross section of ^{16}O (see Fig. 7). This is remarkable considering the light nucleus investigated here and the fact that TALYS is based on statistical models. The apparent overestimation of the experimental results displayed by the theoretical calculation at higher incident energies is explained by TALYS taking into account transitions from higher levels which we were not able to observe with the present setup. Above 14-15 MeV incident energy, where the γ decay is very unlikely (S_p = 12.1 MeV and S_n = 15.6 MeV in ^{16}O [30]), the theoretical curve starts to converge to our results.

The neutron total inelastic cross section of ^{16}O has a total relative uncertainty around 10% for most of the incident energy range (see Fig. 7, panel a). At high energies, where the GELINA neutron flux is small, the statistical component of the total uncertainty starts to dominate leading to a relative uncertainty of 15% at 18 MeV.

B. The ^{16}O(p, pγ)^{16}O reaction

1. *γ-production cross sections*

The main transition

Figure 8 plots the proton inelastic angle-integrated γ-production cross section for the 6128.6-keV transition (E$_{th}$ = 6.5 MeV). All the values for the incident proton energy are given in the laboratory frame of reference and they are average values calculated using the uniform probability distribution function of the proton energy loss inside the target (as explained in Section II C). Other

available experimental data for the same γ ray are also shown. Kiener *et al.* [4] provided the most extensive data set for the proton-induced inelastic channel on ^{16}O: more than 240 cross section points were measured for this transition in the 8.3-20-MeV incident energy range. The same figure also shows the data published by Dyer *et al.* [45]. The very good agreement between the two data sets is due to the fact that the data of Kiener *et al.* for the 6128.6-, 6915.5-, 7115.1- and 2741.5-keV transitions were normalized to the Dyer *et al.* data (see details in Ref. [4]).

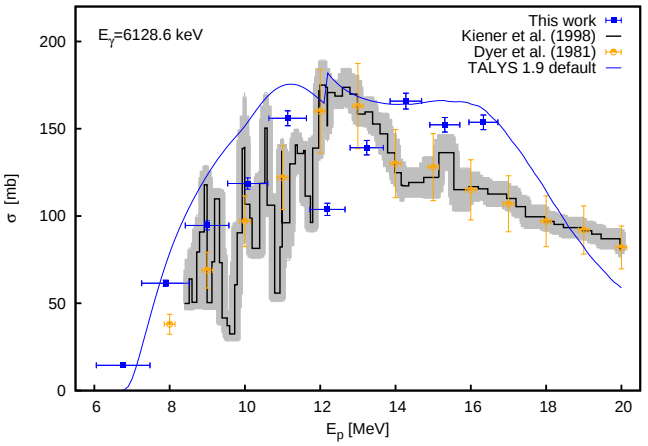

FIG. 8. (Color online) The proton-induced angle-integrated inelastic γ-production cross section for the 6128.6-keV transition in ^{16}O obtained in the present work along with other available experimental data. The TALYS 1.9 model calculations were performed using the default input parameters. Due to the thickness of our target (42.93 mg/cm^2), the cross section points reported here have substantial incident energy uncertainty. In comparison, Kiener *et al.* and Dyer *et al.* used targets with areal densities of only 0.5 and 2.9 mg/cm^2, respectively. The grey band associated to the data of Kiener *et al.* represents the uncertainty.

Except for the very high incident energy region, the overall agreement between the present work and Kiener *et al.* is good considering that our points are actually average cross sections over a relatively large incident energy range (we used a thick target). Complementary to Ref. [4], we provide two more points below 8.3 MeV.

Above 14 MeV, our data points are higher than those of Ref. [4], even though they are consistent with the TALYS prediction in that region. We note that a possible contribution to this γ-production cross section from the ^{16}O(p, n)^{16}F reaction channel followed by β^+ decay of ^{16}F is not possible as ^{16}F decays only through proton emission [30]. The data seems to indicate the presence of a resonance centred around 15.5 MeV and with a width of ≈1.5 MeV.

The TALYS 1.9-default theoretical curve overestimates the experimental data over most of the incident energy range (see Fig. 8). This is especially the case for the dip point at 12 MeV. The near-threshold rise and the overall shape of the cross section is well reproduced by the reaction code.

The higher-lying transitions: 6915.5, 7115.1 and 2741.5 keV

Unfortunately, again owing to the 6877.0-keV contaminant line from ^{28}Si, we were unable to extract a clean cross section for the 6915.5-keV γ ray. Thus, we report here only the properly scaled, summed contribution of the 6915.5- and the 6877.0-keV transitions (see Fig. 9). The authors of Ref. [4] measured more than 50 cross section points in the 8.3-19.9-MeV incident energy range for the 6915.5-keV transition using a target that did not contain silicon. Unsurprisingly, our values lie higher than those reported by Kiener *et al.*

In the 11-20 MeV incident energy region, the TALYS "6915.5 + 6877.0 keV scaled" summed calculation (the blue curve) greatly overestimates the experimental points. However, below 11 MeV, the code is able to describe fairly well the threshold rise of our experimental values.

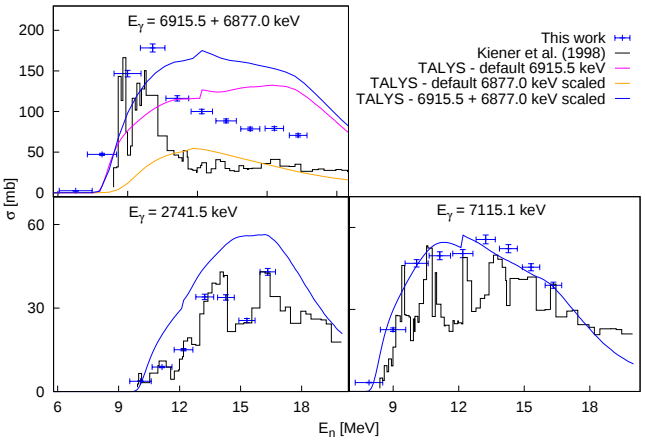

FIG. 9. (Color online) The γ-production cross sections for the higher-lying transitions in ^{16}O extracted in the proton-induced experiment. The data published by Kiener *et al.* is also plotted for all three transitions. Because the 6915.5-keV transition was Doppler shifted to smaller energies ending up on top of the 6877.0-keV transition coming from ^{28}Si (see Section II C), the plot additionally contains also the theoretical calculation for this silicon γ ray. The theoretical calculation labelled "TALYS - 6915.5 + 6877.0 keV scaled" represents the properly scaled, summed cross section of the two transitions.

In the case of the 7115.1-keV γ ray, the TALYS 1.9 curve reproduces our data very well in the entire proton energy range (see Fig. 9). The data of Ref. [4] displays consistently lower values than ours (for example, in the 11-13 MeV proton energy range, it shows a decrease in the reported cross section which is far from both our data and the theoretical calculation).

We were able to measure the cross section for the 2741.5-keV transition with very good statistics (better than 1% statistical uncertainty); this was not the case in the neutron-induced experiment (see Section IV A 1). Due to the very high threshold of this transition (E$_{th}$ = 9.4 MeV), we measured only 7 experimental cross section points in the 10-17 MeV proton energy range (see

Fig. 9). The agreement with the Kiener *et al.* data is very good for the entire incident energy range. An interesting feature can be seen in the 14-16 MeV region, where a pronounced cross section dip is visible in both data sets.

C. The ^{28}Si(p, pγ)^{28}Si reaction data

Figure 10 shows the low-lying levels of ^{28}Si [36]. Even though six transitions coming from the inelastic channel were detected, only four had reasonable statistics and are reported here. The natural abundance of ^{29}Si is 4.68% [1]. This is sufficient to allow parasite contributions in the ^{28}Si γ peaks of interest coming from the ^{29}Si(p, npγ)^{28}Si reaction channel above 10 MeV, which could not be corrected.

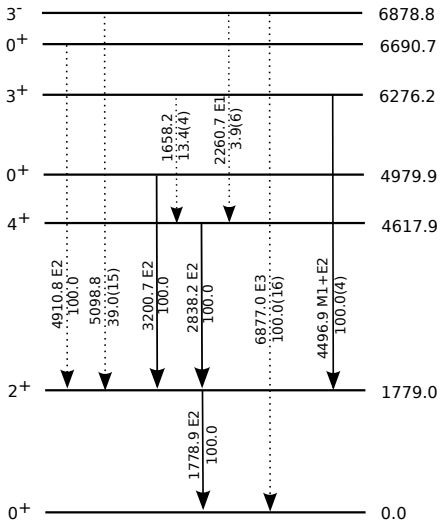

FIG. 10. Partial level scheme of ^{28}Si. In the present experiment we were able to extract the cross section for the transitions drawn with continuous lines.

1. γ-production cross sections

The main transition

The proton-induced inelastic γ-production cross section for the most intense transition in ^{28}Si is given in Fig. 11. The threshold for this transition is at 1.8 MeV. Considering that the Coulomb barrier is $\approx$ 2.3 MeV, the cross section reaches significant values only above 3 MeV.

As mentioned in Section I, proton-induced inelastic data on ^{28}Si is very scarce: a single relatively extended data set is provided by Marchand *et al.* [6], but only for the 3.5-6.6 MeV incident energy range. When compared with our work, the data points by Marchand *et al.* show a good level of agreement, even though the authors of Ref. [6] reported a few very large cross section values

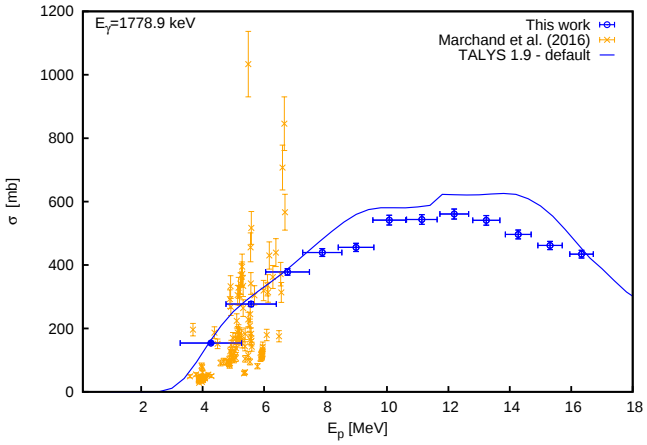

FIG. 11. (Color online) The proton inelastic angle-integrated γ-production cross section for the 1778.9-keV transition in ^{28}Si obtained in the present work with its associated uncertainty. It is compared with other available experimental data and with TALYS 1.9 calculations performed using the default input parameters.

that seem to be caused by a resonant behaviour inaccessible to us. The TALYS 1.9-default theoretical calculation describes our measured points very well, with the exception of the 12-16 MeV incident energy range, where the code shows a small additional contribution which is not confirmed by our experiment.

The higher-lying transitions: 2838.2, 3200.7 and 4496.9 keV

The proton inelastic γ-production cross section for the 2838.2-keV transition in ^{28}Si is shown in Fig. 12. Below 10 MeV, even though TALYS 1.9 describes fairly well the transition's threshold region, the theoretical curve increases faster than the experimental values. In the 12-16 MeV incident energy region for both the 2838.2-keV and 1778.9-keV transitions, the code shows a relatively large contribution which is not confirmed by the experimental data.

Figure 12 also presents our results for the 3200.7- and the 4496.9-keV γ rays, along with their corresponding uncertainty. For both transitions, the TALYS 1.9-default calculation is able to reproduce well the sharp rise of the cross section immediately after the transition's threshold. The same level of agreement is also valid for the high incident energy range, especially for the 3200.7-keV γ ray. At intermediate energies (around 8-13 MeV) the code is less accurate, even though it predicts fairly well the general shape of the cross section.

The experimental cross section points extracted in the proton-induced experiment, for both ^{16}O and ^{28}Si, have a typical uncertainty ranging from 3% up to 10% (see Figs. 8, 9, 11 and 12). These cross section uncertainty differences were generated by the variation of the uncertainty's statistical component from run to run.

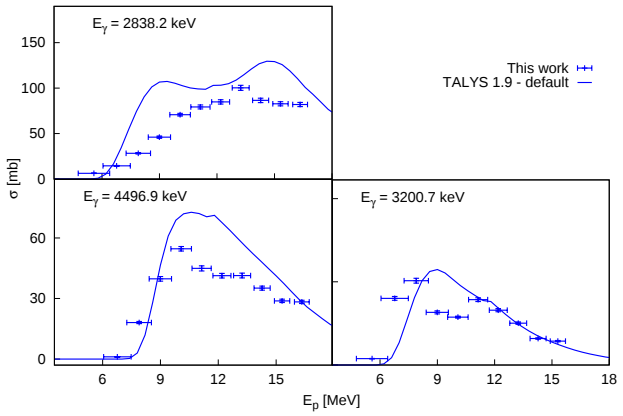

FIG. 12. (Color online) The γ-production cross section for the higher-lying transitions in ^{28}Si extracted in the proton-induced experiment for which no other available angle-integrated γ-production cross sections exist. Thus, our values are compared here only with TALYS-default theoretical calculations.

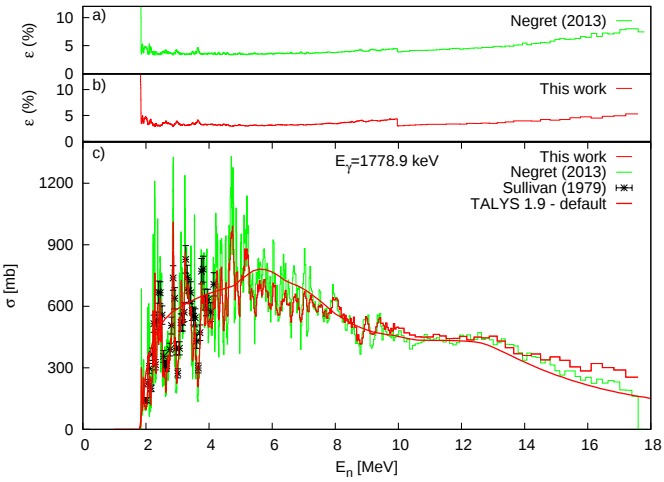

FIG. 13. (Color online) The γ-production cross section of the 1778.9-keV transition obtained during the two neutron-induced experiments on ^{28}Si discussed in the text. Other experimental data for this transition was also plotted [47].

D. Cross-check of our neutron-induced ^{16}O data based on the ^{28}Si(n, nγ)^{28}Si reaction

Our group previously measured the ^{28}Si(n, nγ) cross section using the GAINS spectrometer and an elemental ^{nat}Si sample [16]. This allowed us to perform a cross-check with the present experiment, which employed a SiO_2 target. Figure 13 shows a comparison between the γ-production cross sections for the 1778.9-keV transition in ^{28}Si obtained in the two measurements. The agreement is very good in the entire incident energy range, except for the region above 15-16 MeV.

For the present work, the detector preamplifier gain was changed from 500 mV/MeV to 100 mV/MeV to access the very high γ energies of the ^{16}O nucleus. This setting greatly deteriorated the γ energy resolution, as compared to our previous experiment reported in Ref. [16], leading to the inclusion of two neighbouring peaks when the integration of the 1778.9-keV line of interest was performed during data analysis. Unlike the present work, in the experiment of Negret *et al.* the resolution was sufficiently good to discriminate between these three γ lines. Consequently, the γ-production cross section of the 1778.9-keV transition extracted in the present measurement is contaminated in the entire incident energy range by two neighbouring γ peaks. However, this contamination causes a noticeable difference in respect to Ref. [16] only above 15 MeV, where the cross section for the 1778.9-keV transition decreases and becomes comparable to the one for the other two neighbouring peaks. The complete discussion of the ^{16}O data cross-check is given in Refs. [27, 46].

After taking under consideration the above observations, the overall agreement between the two data sets supports the claimed reliability of the cross sections measured at the GELINA using the GAINS spectrometer.

V. DISCUSSION OF THE NEUTRON- VERSUS PROTON-INDUCED REACTION DATA ON ^{16}O AND ^{28}SI

As mentioned in Section I, our main motivation for measuring neutron- and proton-induced reactions on the same nuclei is related to the possibility of inferring the neutron inelastic cross section from the corresponding proton one. This section discusses various aspects of the comparison between the proton and the neutron inelastic reactions leading to the development of a procedure which is able to relate the two cross sections. This procedure is further applied to the particular case of the ^{16}O and ^{28}Si target nuclei.

A. Reaction mechanisms

Figure 14 displays a comparison between the neutron and proton inelastic γ-production cross sections measured in the present work together with the default TALYS calculation. The effect of the Coulomb barrier is to decrease the reaction probability mainly in the first few MeV after the threshold, which translates into a smaller cross section for protons. This effect is more prominent for the ^{28}Si target.

Overall, the two projectiles excite similar structures in the compound mirror nuclei (CN) through which the reactions proceed. This is to be expected considering the similarity that exists between the neutron- and proton-target OMPs and between the nuclear structure of mirror nuclei (both are due to isospin symmetry). In the context of the present study, it is instructive to investigate the interplay between the different reaction mechanisms involved in the incident energy range of interest for the inelastic channel on ^{16}O and ^{28}Si (2-20 MeV), along with

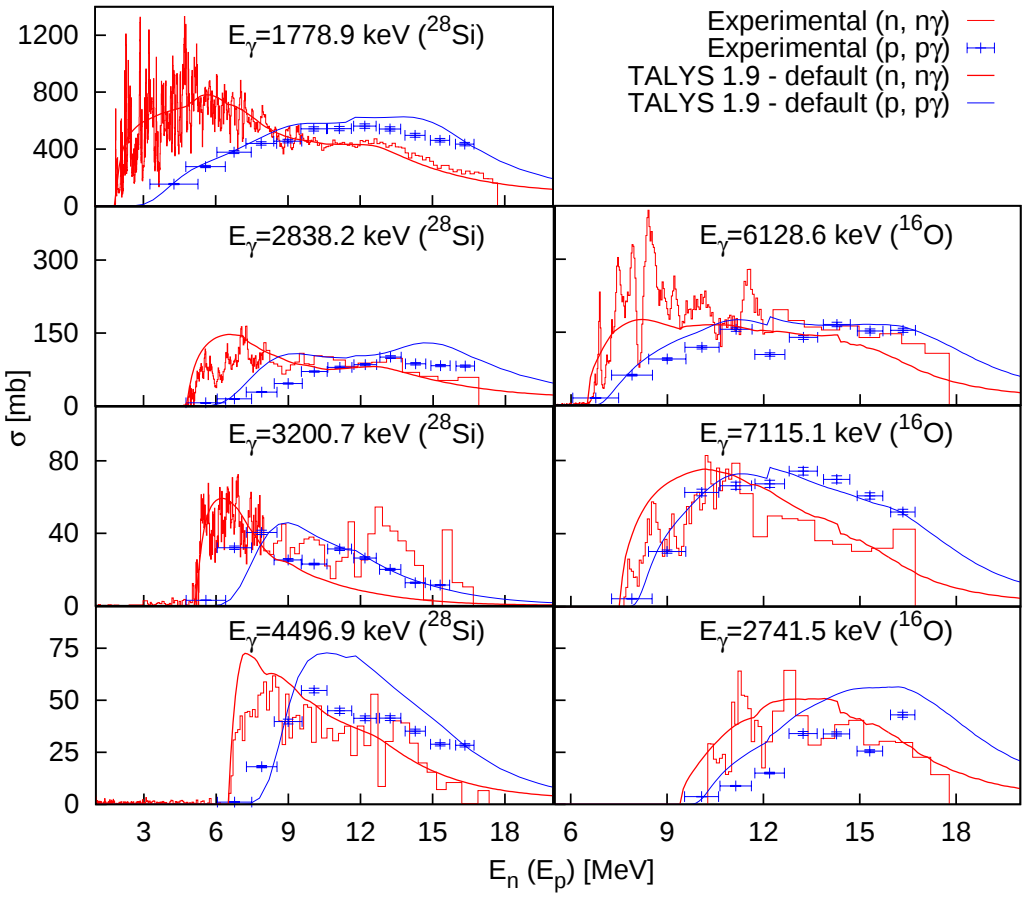

FIG. 14. (Color online) Comparison between the neutron- and proton-induced inelastic γ-production cross sections measured in the present work together with the corresponding TALYS 1.9-*default* calculations.

the possible mismatch between the excitation energies, spins and parities being populated in the CN by the two projectiles.

The compound nucleus mechanism determines a fluctuating behaviour of the measured cross section due to the CN resonances [48]. The pre-equilibrium and direct mechanisms display a rather smooth variation with the incident energy and are expected to play a significant role only at high energies (>15-20 MeV). Figure 15 shows the contribution of each reaction mechanism as a function of the incident energy for the neutron and proton cases, according to TALYS 1.9. The compound nucleus mechanism dominates only up to around 15 MeV. This is actually helpful in our case because a smaller contribution from this reaction mechanism reduces the dependence on the structural differences between the two compound mirror nuclei (^{17}O-^{17}F and ^{29}Si-^{29}P) corresponding to the inelastic reactions investigated in the present work. The dependence of the present approach on the nuclear structure-related effects is discussed in more detail in the next two sub-sections.

Figure 16 shows that, according to TALYS, the two projectiles populate CN states with very similar angular momenta and parities J^π. The proton and neutron

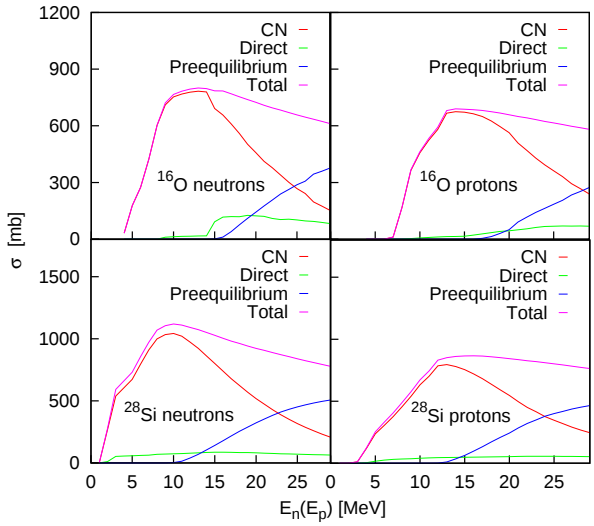

FIG. 15. (Color online) The contribution of each reaction mechanism (CN, direct and pre-equilibrium) to the total reaction cross section (which includes the inelastic channel) in the 0.1-30 MeV incident energy range, as given by TALYS 1.9-default calculations.

distributions are practically identical at 15 MeV while this is not the case at 5 MeV. This indicates that the Coulomb term from the projectile-target OMP plays a relevant role only at small incident energies. The electromagnetic interaction is also responsible for the somewhat larger asymmetry between the neutron- and proton-induced distributions (especially at 5 MeV) in the case of ^{28}Si, as compared to ^{16}O.

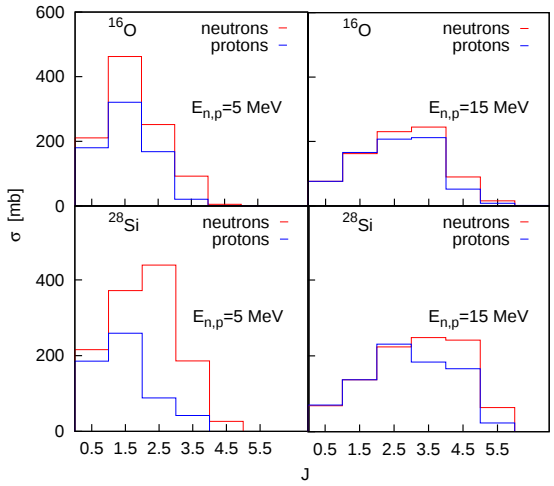

FIG. 16. (Color online) The total angular momentum and parity J^π populated in the compound nucleus by 5 MeV (15 MeV) incident neutrons and protons in the case of the ^{16}O and ^{28}Si targets. The plotted values were extracted from a TALYS 1.9-default calculation. The code's output consists of separate angular momenta values for the negative and the positive parity states, so, we simply added the two to obtain the values plotted here.

The Hauser-Feshbach theory of CN reactions supposes that the reaction dynamics mainly depends on the excitation energy, the spin and the parity of the CN state [7, 48]. However, it is very helpful to assume that, in a first approximation, the decay of the CN states only depends on the available excitation energy. This is known as the Weisskopf-Ewing limit [7, 48] of the Hauser-Feshbach theory and it works best for reasonably high excitation energies (above 20 MeV [7]). In order to work in the excitation energy regime where this approximation holds best, all the surrogate-reactions studies employed reactions at relatively high incident energies, where the direct reaction mechanism dominates [7–14].

An important difference between the present and the surrogate approach is that we do not investigate two reactions that proceed through *the same* CN, hence we are not limited by the validity of the Weisskopf-Ewing approximation. In any case, this would not be a stringent issue in our approach because the neutron and proton populate very similar angular momenta and parities J^π in the CN (as shown in Fig. 16). We investigate the inelastic channel, hence the reactions of interest are modelled at relatively low incident (and excitation) energy where the CN dominates. This is not the case for the direct reactions employed in the surrogate studies.

We point out that, due to the difference between the neutron (S_n) and proton (S_p) separation energy in their respective compound mirror nuclei, there is a difference in the excitation energy populated by the two projectiles. For example, in the case of the ^{28}Si target, this difference can be calculated using [49]:

$$S_n(^{29}Si) - S_p(^{29}P) = 8473.6 - 2749.0 = 5724.6\ keV \quad (4)$$

Similarly, for the ^{16}O target:

$$S_n(^{17}O) - S_p(^{17}F) = 4143.8 - 600.2 = 3543.6\ keV \quad (5)$$

The above values show that, at *the same* incident energy, the neutron always populates CN excited states that are 5724.6 keV and 3543.6 keV higher than the corresponding proton reaction for the ^{28}Si and ^{16}O targets, respectively. Evidently, this will induce differences between the neutron and proton reaction dynamics.

Due to isospin symmetry, mirror nuclei have similar nuclear structure because the Coulomb term in the (phenomenological) shell model potential only slightly modifies the shape of the proton potential, as compared with the neutron one (for low enough Z values) [50, 51]. Moreover, as soon as higher excitation energy CN single-particle states are being accessed in the continuum (by increasing the incident energy), the shape of the shell model potential becomes increasingly similar in the proton and neutron cases and, consequently, so do the values of the quantum observables associated to these single-particle orbitals. This is the main nuclear structure-related reason for the observed similarities between the experimental neutron- and proton-induced inelastic cross sections reported in this work, especially at higher incident energies (see Fig. 14). The other important reason has to do with the projectile-target OMP similarities. This point is discussed below.

B. The proton- and neutron-target OMPs

In the study from Ref. [16] Negret *et al.* compared the ^{28}Si(n, nγ)^{28}Si and the ^{25}Mg(α, nγ)^{28}Si reactions, which proceed through the same CN and, due to the different projectile-target combination, are modelled by fairly distinct OMPs. These differences were further enhanced by the non-identical ground state spin of the two targets (0^+ and $5/2^+$ in the case of ^{28}Si and ^{25}Mg, respectively). Ideally, if the excitation energy is high enough, these differences should be significantly diminished by the "no memory" property of the CN reactions [7, 17]. In reality, many relevant differences remained mainly due to the low excitation energy range associated to the inelastic channel studied in Ref. [16] (i.e. the Weisskopf-Ewing approximation is not valid in this low excitation energy regime).

To avoid such issues, in the present study we used very similar projectiles and identical $N = Z$ target nuclei so that the corresponding neutron- and proton-target OMPs were practically the same, up to the parametrisation employed in the two cases. More precisely, we made use of the OMP implemented by the TALYS 1.9 reaction code, for both incident neutrons and protons ([31] and the references therein):

$$U(r,E) = -V_V(r,E) - iW_V(r,E) - iW_D(r,E) + V_{SO}(r,E)\cdot l\cdot\sigma + iW_{SO}(r,E)\cdot l\cdot\sigma + V_C(r) \quad (6)$$

where $U(r,E)$ is the neutron- (or proton-) target OMP and $V_{V,SO}$ and $W_{V,D,SO}$ are the real and imaginary components of the volume (V), surface (D) and spin-orbit (SO) terms, respectively. The energy E of the incoming projectile is given in the LAB reference frame. The Coulomb term $V_C(r)$ is missing for incident neutrons. Each term from above is separated into an energy-dependent well depth $[V_V(E), W_V(E), W_D(E), W_{SO}(E)]$ and an energy-independent radial part that contains the geometrical parameters of the target nucleus (i.e. the usual Woods-Saxon shape). The local and/or global parametrisations associated to the neutron and proton phenomenological OMPs employed by TALYS for ^{16}O and ^{28}Si are detailed in the code's manual.

Equation (6) shows that, from a formal point of view, the only difference between the neutron and proton OMPs employed by TALYS is given by the Coulomb term V_C and by the opposite sign of the Lane term [which is proportional to $(N-Z)/A$ and is part of the potential depth $V_V(E)$] [31, 52, 53]. Within the Lane model, a small isospin dependence of the real part of the OMP is postulated. Due to nuclear pairing, the isospin-generated couplings are the strongest in $N = Z$ nuclei [50, 51], and hence the use of Lane-consistent OMPs is helpful in the present study. This type of potentials allows [through the $(N-Z)/A$ asymmetry term] a systematic investigation of both $N = Z$ and $N \neq Z$ target nuclei.

The differences between the neutron- and proton-induced reactions on the same target nucleus are generated in essence by three causes: the electromagnetic interaction, the nuclear structure of the CN and the very small isospin asymmetry between the two projectiles (even without the Coulomb interaction, the neutron and proton are not identical if we consider their internal structure as described by Quantum Chromodynamics [54]). Amongst all these differences, the electromagnetic effects have the biggest impact on the neutron- versus the proton-induced cross sections and they can be quantified by inserting a Coulomb term V_C for protons into the OMP. An important observation is that, because the CN reaction mechanism dominates at low incident energies, the inelastic channel has the highest sensitivity to the nuclear structure of the CN when compared to the other non-elastic reactions (which occur predominantly in the pre-equilibrium and direct reactions regime). Hence, any important structural difference between the two compound mirror nuclei associated to the proton and neutron reactions on the same target will generate differences between the induced inelastic cross sections and these should be carefully addressed in the context of the present study. Finally, the small isospin asymmetry between the two nucleons is quantified, as mentioned, by assuming a small isospin dependence of the OMP [52, 53] and this asymmetry can be managed by simply inverting the sign of the Lane term when going from the proton to the neutron optical potential.

C. The procedure used to infer the (n, nγ) cross sections from the (p, pγ) data

As already stated, the main goal of this section is to investigate to which extent it is possible to infer the neutron-induced inelastic cross sections from the corresponding proton ones in the case of ^{16}O and ^{28}Si. By exploiting the above-mentioned similarities between the proton and the neutron OMPs, one can use the following procedure consisting of 3 steps:

1. One measures the proton-induced inelastic cross section for all the observed transitions coming from ^{16}O and ^{28}Si.

2. Reaction calculations are performed using TALYS; the theoretical default curve is fitted until an acceptable agreement is reached with the experimental proton-induced cross sections (obtaining the green curve from Fig. 17).

3. Using the proton OMP from the previous step, the V_C term is set to zero and the sign of the Lane term is inverted, allowing one to extract a neutron-like OMP from the corresponding proton one. By performing calculations using this neutron-like OMP + incident *protons*, one can then generate neutron-like inelastic cross sections - the black curve from Fig. 17. In our particular case of $N = Z$ targets the Lane term is obviously zero.

Figure 17 displays the results we extracted using this procedure for all the reported transitions in ^{16}O and ^{28}Si (except the 6915.5-keV γ ray). The "TALYS 1.9 - tuned (p, pγ)" curves (in green) were obtained by tuning proton OMP parameters separately for each transition to generate optimized descriptions of the experimental proton scattering cross sections. In the case of the 6128.6-, 7115.1- and 1778.9-keV γ rays, the parameter modifications were small (3-7%). However, considering the poor agreement between the default calculation and the experimental proton-induced cross section for the 2741.5-, 2838.2- and 3200.7-keV transitions (see Fig. 14), for these γ rays the required parameter modifications were significant (15-36%). Unfortunately, in the case of the 4496.9-keV γ ray the modifications needed for reaching a reasonable agreement between the theoretical calculation and the experimental points were larger than 50%.

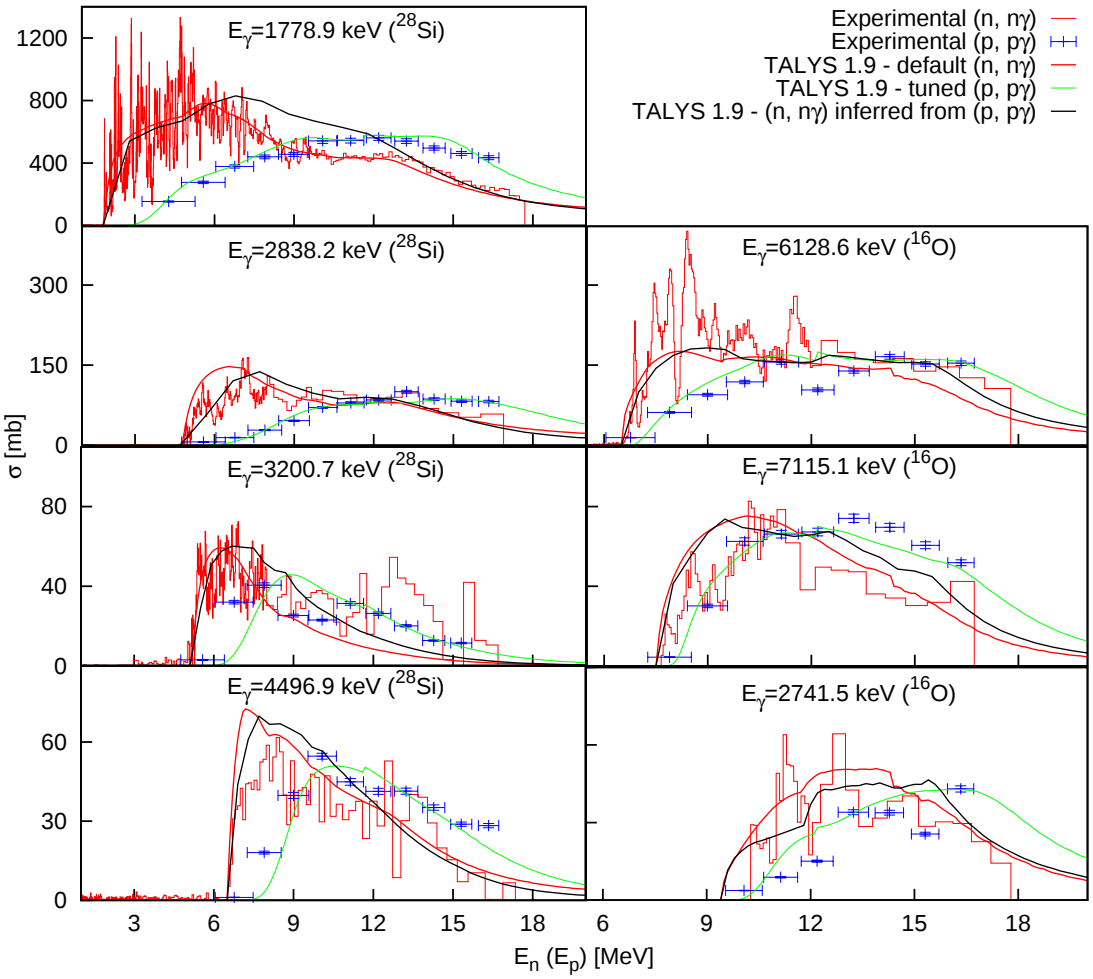

FIG. 17. (Color online) The results of the present investigation for the ^{16}O and ^{28}Si transitions. The proton-induced experimental and theoretical-*tuned* cross section values are displayed in blue and green, respectively, while the neutron-induced experimental and theoretical-*default* are given in red. The calculation corresponding to the black curve was obtained from the green one using a *proton* OMP that had no V_C term and an inverted sign of the Lane term (as described in the main text). All theoretical values were calculated using the versatility offered by the TALYS 1.9 reaction code.

Consequently, in this case we simply re-scaled the default calculation from Fig. 14 to obtain the "TALYS 1.9 - tuned (p, pγ)" green curve. We mention that the same re-scaling factor was used when generating the corresponding neutron-induced inelastic cross section. Further, by dropping the V_C term and inverting the Lane term's sign of the proton OMP corresponding to the "TALYS 1.9 - tuned (p, pγ)" green curve, we calculated for each transition the "TALYS 1.9 - (n, nγ) inferred from (p, pγ)" black curve (see Fig. 17).

As a general remark, in the vicinity of the transition threshold, the agreement between the "TALYS 1.9 - default (n, nγ)" red curve and the "TALYS 1.9 - (n, nγ) inferred from (p, pγ)" black curve obtained via the above procedure is very good; in this incident energy region, for many transitions, the "TALYS 1.9 - (n, nγ) inferred from (p, pγ)" calculation actually describes better the neutron-induced experimental points than the "TALYS 1.9 - default (n, nγ)" one (see especially the case of the 2838.2- and 2741.5-keV γ rays). Also, at very high incident energies, where the Coulomb effects become very small, the calculation in which the V_C term was set to zero better predicts in general the neutron experimental points as compared with the "TALYS 1.9 - default (n, nγ)" red curve. Overall, the procedure seems to work better for ^{16}O than for ^{28}Si, again suggesting that the observed differences are mostly electromagnetic (and not structural).

For all transitions we observe that in general the "TALYS 1.9 - (n, nγ) inferred from (p, pγ)" calculation - obtained from the "TALYS 1.9 - tuned (p, pγ)" one by dropping the V_C term - is able to better describe the experimental neutron-induced cross sections as compared with the same procedure be done starting from the "TALYS 1.9 - default (p, pγ)" curve displayed in Fig. 14. In some cases the improvement was substantial (see the 2838.2-keV transition, for example). This is understandable because the "TALYS 1.9 - tuned (p, pγ)" employed

tuning the default theoretical calculation to better match the experimental (p, p') data. Also, this indicates that the procedure we use to generate the (n, n') cross sections is valid.

In several cases however, a significant difference is visible in the 8-13 MeV range between the experimental (n, nγ) data and the black curve inferred from the (p, pγ) reactions (see, for instance, the 1778.9-keV transition but also the other ^{28}Si transitions from Fig. 17). The disagreement starts around the threshold for other important reaction channels [(p, 2p), (p, α)...] and has an obvious reason: unfortunately, when we drop the V_C term for incident protons, this also influences all the other exit channels that evaporate protons from the CN. These Coulomb-related changes of the other non-elastic reactions, in turn, modify (via the total cross section) the inelastic channel. Therefore, these and other consequences of removing the V_C term should be carefully addressed for a further improvement of this procedure. Also, one should keep in mind that such effects could become more important in heavier nuclei, hence more challenging.

To summarize, using the experimental proton-induced reaction data, we showed that a fairly reliable neutron-like OMP can be determined. This optical potential seems to acceptably model the neutron total reaction cross section by reasonably assessing the absorbed incident flux. The reaction cross section includes the inelastic channel, hence, this neutron-like OMP allows for an acceptable description of the experimental neutron-induced inelastic cross section. The current work shows encouraging results suitable for further developments to enhance the agreement for the inelastic channel, in particular. We mention, however, that a more consistent approach on the relation between the (n, n') and (p, p') cross sections implies studying also other target nuclei: ^{24}Mg, ^{40}Ca, ^{57}Fe, ^{58}Ni, etc. In this context, several relevant issues are still to be addressed:

- the unfortunate Coulomb-related effects in the outgoing channels caused by the removal of the V_C term.
- the influence of the Lane term for $N \neq Z$ targets.
- the role played by the nuclear structure effects when the CN corresponding to the proton and neutron reactions are no longer mirror nuclei.

All these issues may become more challenging for heavier targets.

VI. CONCLUSIONS

This work reports measurements of neutron and proton inelastic scattering cross sections of ^{16}O and ^{28}Si using SiO_2 targets. The neutron beam experiment was performed at the GELINA facility using the GAINS spectrometer while the proton beam one employed the 9-MV Tandem Accelerator of IFIN-HH. The angle-integrated γ-production inelastic cross sections for eight transitions are reported with an uncertainty smaller than 6% for the most intense γ rays. By making use of the γ-production cross sections, the total inelastic cross section was also determined. Our results were compared with other experimental values and with TALYS 1.9 calculations. The comparison shows a very good agreement, especially in the case of the neutron beam experiment.

The second part of this paper presents a comparison of the neutron and proton inelastic cross sections. Another goal of this work was to study if and to which extent the neutron-induced inelastic cross sections on ^{16}O and ^{28}Si can be related to those obtained using proton-induced reactions. In doing so, one exploits the isospin symmetry by using $N = Z$ nuclei as targets and, consequently, forming mirror compound nuclei in the (n, n') and (p, p') reactions. We showed that, by making use of the great formal similarities between the neutron- and the proton-target OMPs and of the isospin symmetry in mirror nuclei, one can employ a procedure that combines experimental proton-induced inelastic cross sections with state-of-the-art theoretical calculations to infer neutron inelastic cross sections on ^{16}O and ^{28}Si from the proton corresponding ones with a 10-20% precision.

While other studies of this kind were already performed for the (n, fission), (n, γ) and, quite recently, also for the (n, p) reactions - using different approaches than the present one - this is the first time when such an investigation is done for the neutron inelastic channel. We plan to further develop our results by systematically investigating also other target nuclei: ^{24}Mg, ^{40}Ca, ^{58}Ni, ^{57}Fe, etc. It will be interesting to see what results will our study yield for heavier, $N \neq Z$ target nuclei. For this type of nuclei, this investigation will allow to better understand what is, among others, the dependence of this procedure on the Lane term, as compared to the $N = Z$ case studied in the present work where this term is zero.

ACKNOWLEDGMENTS

This work was supported by the European Commission within the Seventh Framework Programme through Fission-2013-CHANDA (project no. 605203) and EUFRAT (project no. 211499) and by the Ministry of Research and Innovation of Romania, CNCS-UEFISCDI, through the project number PN-III-P4-ID-PCE-2016-0025 within PNCDI III and through the PN19060102 project. Partial support was also offered by the 16-ELI-RO-2016 and 13-ELI-RO-2017 research grants. M. Boromiza acknowledges the POSDRU scholarship (POSDRU/159/1.5/S/137750) for PhD and Posdoctoral students of the Bucharest University, Romania. We further like to show our gratitude towards the support team of the GELINA facility and of the 9-MV Tandem Accelerator (IFIN-HH) for providing good quality beams during the two experiments.

[1] J. Meija, T.B. Coplen, M. Berglung, W.A. Brand, P. De Bievre, M. Groning, N.E. Holden, J. Irrgeher, R.D. Loss, T. Walczyk, and T. Prohaska, Pure and Applied Chemistry, 88, 293 (2016).

[2] M. Chadwick *et al.*, Nuclear Data Sheets, 148, 189-213 (2018).

[3] Nuclear Data High Priority Request List: http://www.oecd-nea.org/dbdata/hprl/, ^{16}O entry.

[4] J. Kiener, M. Berheide, N. Achouri, A. Boughrara, A. Coc, A. Lefebvre, F. Santos and C. Vieu, Physical Review C, 58, 4 (1998).

[5] N. Otuka, Towards a More Complete and Accurate Experimental Nuclear Reaction Data Library (EXFOR): International Collaboration Between Nuclear Reaction Data Centres (NNDC), Nuclear Data Sheets, 120, 272-276 (2014).

[6] B. Marchand, K. Mizohata, and J. Risnen, Nuclear Instruments and Methods in Physics Research B, 378, 25-30 (2016).

[7] J.E. Escher, J. T. Burke, F.S. Dietrich, and N.D. Scielzo, Reviews of Modern Physics 84, 353, (2012).

[8] C. Plettner, Physical Review C, 71, 054602 (2005).

[9] J. Burke, Physical Review C, 73, 054604 (2006).

[10] B. Goldblum, Physical Review C, 78, 064606 (2008).

[11] M. Petit, Nuclear Physics A, 735, 345 (2004).

[12] S. Boyer, Nuclear Physics A, 775, 175 (2006).

[13] J. Allmond, Physical Review C, 79, 054610 (2009).

[14] S. Chiba, and O. Iwamoto, Physical Review C, 81, 044604 (2010).

[15] B. Pandey, Physical Review C, 93, 021602(R) (2016).

[16] A. Negret *et al.*, Physical Review C, 88, 034604 (2013).

[17] A. Bohr and B. Mottelson, Nuclear Structure, World Scientific Publishing Co. Pte. Ltd., New York, 492 (1998).

[18] W. Mondelaers and P. Schillebeeckx, Notiziario neutroni e luci di sincroton, 11, 19-25 (2010).

[19] D. Deleanu, C. Borcea, P. Dessagne, M. Kerveno, A. Negret, A.J.M. Plompen, and J.C. Thiry, Nuclear Instruments and Methods in Physics Research A, 624, 130 (2010).

[20] A. Olacel, C. Borcea, P. Dessagne, M. Kerveno, A. Negret, and A.J.M. Plompen, Physical Review C, 90, 034603 (2014).

[21] A. Olacel, C. Borcea, M. Boromiza, P. Dessagne, G. Henning, M. Kerveno, L. Leal, A. Negret, M. Nyman, and A.J.M. Plompen, European Physical Journal A, 54:183 (2018).

[22] C. Rouki *et al.*, Nuclear Instruments and Methods in Physics Research A, 672, 82 (2012).

[23] D. Bucurescu, G. Cata-Danil, and N.V. Zamfir, Nuclear Physics News, 17, 5 (2007).

[24] S. Dobrescu, D.V. Mosu, D. Moisa, and S. Papureanu, AIP Conference Proceedings No. 1099 (2009).

[25] L. Arnold *et al.*, TNT digital pulse processor, Proceedings of Real Time Conference, 14th IEEE-NPSS, 1547443, 265-269 (2005).

[26] X-6 Monte Carlo Team, MCNP - A general N-particle transport code, version 6, Volume I: overview and theory, Los Alamos National Laboratory, http://laws.lanl.gov/vhosts/mcnp.lanl.gov.

[27] M. Boromiza, Nucleon inelastic scattering cross sections on ^{16}O and ^{28}Si, University of Bucharest, Romania, PhD thesis (2018).

[28] M. Boromiza, C. Borcea, A. Negret, A. Olacel, and G. Suliman, Nuclear Instruments and Methods in Physics Research A, 863, 15-19 (2017).

[29] C. Mihailescu, Neutron (n, xnγ) cross sections measurements for ^{52}Cr, ^{209}Bi and ^{206,207,208}Pb from threshold up to 20 MeV, European Commission Joint Research Center Geel, Belgium, PhD thesis (2006).

[30] D.R.Tilley, H.R.Weller, and C.M.Cheves, Nuclear Physics A, 564, 1 (1993).

[31] A. Koning, S. Hilaire, and M Duijvestijn, Proceedings of the International Conference on Nuclear Data for Science and Technology, EDP Sciences, 211, 1, Nice, France (2007).

[32] http://www.srim.org/.

[33] C. Mihailescu, C. Borcea, and A.J.M. Plompen, Nuclear Instruments and Methods in Physics Research A, 578, 298-305 (2007).

[34] K.E. Atkinson, An introduction to numerical analysis, John Wiley and Sons, New York, 712 pages (1989).

[35] A. Carlson *et al.*, Nuclear Data Sheets, 110, 3215 (2009).

[36] M. Basunia, Nuclear Data Sheets, 114, 1189 (2013).

[37] M. Boromiza *et al.*, Proton inelastic scattering cross section measurements on ^{16}O and ^{28}Si, Proceedings of the International Conference on Nuclear Data for Science and Technology, Bruges, Belgium, EPJ Web of Conferences, 146, 11015 (2016).

[38] R. Nelson, M. Chadwick, A. Michaudon, and P. Young, Nuclear Science and Engineering, 138, 105-144 (2001).

[39] J. Dickens and F. Perey, Nuclear Science and Engineering, 40, 283 (1970).

[40] V. Orphan, C. Hoot, and J. John, Nuclear Science and Engineering, 42, 352 (1970).

[41] V. Besotosnyj, V. Gorbachev, L. Suvorov, and M. Shvecov, Rept: Yadernye Konstanty, 19, 77 (1975).

[42] M. Chadwick, Nuclear Data Sheets, 112, 2011 (2007).

[43] Z. Ge, Z. Zhao, H. Xia, Y. Zhuang, T. Liu, J. Zhang, and H. Wu, Journal of Korean Physical Society 59, No. 2, 1052 (2011).

[44] A. Santamarina, D. Bernard, and Y. Rugama, JEFF Report 22 (2009).

[45] P. Dyer, D. Bodansky, A. Seamster, E. Norman, and D. Maxson, Physical Review C, 23, 5 (1981).

[46] M. Boromiza, C. Borcea, P. Dessagne, G. Henning, M. Kerveno, A. Negret, M. Nyman, A. Olacel, and A. Plompen, High precision neutron inelastic cross sections on ^{16}O, Proceedings of the International Conference on Nuclear Data for Science and Technology, Beijing 2019, to be published.

[47] N. Sullivan, J. Egan, G. Kegel, and P.Harihar, Nuclear Science and Engineering, 70, 294 (1979).

[48] W. Hauser and H. Feshbach, Physical Review C, 87, 366-373 (1952).

[49] M. Wang, G. Audi, F. Kondev, W. Huang, S. Naimi, and X. Xu, The Ame2016 atomic mass evaluation (II), Chinese Physics C, 41, 030003 (2017).

[50] G. Vladuca, Elemente de fizica nucleara Vol. II, Bucuresti (1988).

[51] P. Ring and P. Schuck, The nuclear many-body problem, Springer-Verlag, Berlin, Germany (1980).

[52] A. Lane, Nuclear Physics, 35, 676-685 (1962).

[53] A. Lane, Physical Review Letters, 8, 4 (1962).

[54] W. Greiner and A. Schafer, Quantum Chromodynamics, Springer-Verlag, second edition, New York (1994).